Microstructure, isothermal and thermomechanical fatigue behaviour of leaded and lead-free solder joints

Mohammad Ghaleeh[1], Ahmad Baroutaji[2(*)], Mansour Al Qubeissi[3]

[1] Department of Engineering, University of Northampton, Northampton NN1 5PH, UK

[2] School of Engineering, University of Wolverhampton, Telford Innovation Campus, TF2 9NT, UK

[3] School of Mechanical, Aerospace and Automotive Engineering, Faculty of Engineering, Environment and Computing, Coventry University, Coventry CV1 2JH, UK

Abstract

The reliability of solder joints is a critical issue in the microelectronics industry. The requirement of permanent electrical and thermal connections between solder alloys and the various components of a surface mount device is dependent upon the mechanical integrity of the solder and its interfaces.

Accordingly, in this paper, the reliability of lead-free, Sn-3.8Ag-0.7Cu, and leaded, Sn-37Pb, solder alloys was investigated under both thermal-mechanical fatigue (TMF) and isothermal mechanical fatigue (IF) conditions. The investigation included material characterisation and fatigue testing on 4-ball grid array (BGA) specimens. The IF tests were carried out under load control at three different temperatures including Room Temperature (RT), 35°C and 75°C. Also, a set of 'not-in-phase' (nIP), 'in-phase' (IP) and 'out-of-phase' (OoP) combined thermal and mechanical cycling tests were carried out to investigate the TMF behaviour of the solders. The stress-life curves for each test condition were generated and then compared taking into account the observations on microstructure.

It was found that the IF and TMF performance of Sn-3.8Ag-0.7Cu alloy was better than Sn-37Pb alloy when expressed as stress-life curves. Additionally, the Sn-3.8Ag-0.7Cu was less susceptible to the changes in temperature. This study provides a comprehensive insight into the reliability of solder alloys under a wide range of loading conditions.

[*] **Corresponding author**
Dr Ahmad Baroutaji
School of Engineering, University of Wolverhampton, Telford Innovation Campus, Priorslee, Telford, TF2 9NT, UK Tel: +44 (0)1902 322981; fax: +44 (0)1902 323843
E-mail address: ahmad.baroutaji2@mail.dcu.ie

Keywords: Solder joints, Lead-free, shear stress, Ball Grid Array, Thermo-mechanical fatigue, isothermal fatigue.

1. Introduction

The ever-growing demand for greater packaging density with high performance is being met with surface mount technologies (SMT) such as flip-chip and ball grid arrays (BGAs). Such technologies, i.e. SMT, involve an increase in the number of solder joints per package and a reduction in joint dimensions but they lead to the formation of complex heterogeneous microstructures within the solder joints. So understanding the microstructure and mechanical behaviour of solder joints with small size has become critical in determining the overall reliability of interconnections [1–6].

Tin-lead (Sn-Pb) based solders have traditionally been used in the microelectronics industry due to their relatively low melting point, good mechanical properties, eutectic characteristic (good freezing behaviour), fine microstructure (giving good strength), low cost, easy manufacturability, and good wetting of common substrates, such as Cu and Ni. Such characteristics make eutectic or near eutectic Sn-37Pb alloys well suited to electronics applications. However, environmental and health concerns led to the banning of leaded solder alloys from 2006 under the European Commission's (EC) directives, Waste Electrical and Electronic Equipment (WEEE) and Restriction of Hazardous Substances (ROHS). This, and similar initiatives worldwide, make the advent of lead-free electronics inevitable [7]. Among the different lead-free solders, Sn-Ag-Cu (SAC) solder alloys were the most used one by industry [8].

In addition to the thermal loading generated during the work of the electronic device, electronic assemblies can be subjected to cyclic mechanical loading from different sources such as vibration or bending of structures to which they are mounted. Various investigations have been conducted to study the thermal and thermal-mechanical fatigue behaviour of lead-tin [9–11] and lead-free [12–14] solders. Wiese et al. [15] constructed a mechanical fatigue

tester and observed the behaviour of 95.5Sn-4Ag-0.5Cu and Sn-37Pb solder joints using an SEM during mechanical cycling experiments at room temperature with strain ranges from 0.3% to 4%, at frequencies from 0.0004 Hz to 10Hz. The results showed that the crack propagation rate of 95.5Sn-4Ag-0.5Cu solder joints is greater than that for Sn-37Pb, at room temperature. Park and Lee [16,17] applied loading conditions varying from tensile to pure shear on Sn-3.5Ag-0.75Cu and Sn-37Pb solder joints. The results revealed that the fatigue life increased with increasing the loading angle, i.e. loads change from pure tension to pure shear. Lee et al. [18] have carried out similar low cycle fatigue tests to characterise the fatigue behaviour of Sn-3.5Ag, Sn-3.5Ag-Cu, Sn-3.5Ag-Bi, and Sn-0.7Cu joints at room temperature. Zhang et al. [19] characterised the isothermal mechanical durability of three lead-free solders including Sn-3.9Ag-0.6Cu, Sn-3.5Ag, and Sn-0.7Cu, and compared with those of the eutectic Sn-37Pb solder at the room temperature and at 135°C. The authors observed that the Sn-3.9Ag-0.6Cu and Sn-3.5Ag had much better durability than the Sn-37Pb, while the Sn-0.7Cu was worse. Cuddalorepatta et al. [20] studied the effects of cyclic loading damage accumulation on the elastic-plastic properties of lead- free solder joints (Sn-3.0Ag-0.5Cu). They found that initial elastic, plastic and yield properties decreased with increasing damage and that the rate of decrease was proportional to the load severity. Kanda et al. [21] investigated the effect of waveform symmetry on the low cycle fatigue of lead-free solder joints (Sn-3.8Ag-0.5Cu). They showed that the symmetry of triangular waves had no significant effect on crack initiation or life for lead-free micro specimens, in contrast to the reductions observed for large size specimens. Peng et al. [22,23] determined the Coffin-Manson constants for the low cycle fatigue life of Sn-8Zn-3Bi solder joints, using Sn-37Pb eutectic as a reference. Duek et al. [24] carried out low cycle isothermal fatigue tests on 96.5Sn-3.0Ag-0.5Cu solder joints at 24°C, 30°C, 60°C, 100°C, and 125°C with fixed constant displacement amplitude. The obtained results revealed that the crack growth is slower at higher temperature with slow mechanical loading and that the fatigue life increased with increasing the temperature. Di Maio et al. [25] characterised the fatigue properties of 96.5Sn-3.0Ag-0.5Cu solder joints. Isothermal tests were carried out at 40°C and 125°C with and

without applying a current density. It was found that the specimens subjected to high current failed faster than those without.

Many investigators have examined the effect of temperature on isothermal low-cycle fatigue. Kanchanomai and Moutoh [26] examined the temperature effects on the low cycle fatigue of 96.5Sn-3.5Ag specimens at three different temperatures 20, 85, and 120°C. They observed that the fatigue life decreased with an increase in temperature but that the plastic strain range increased meaning that the stress range decreased. Korhonen et al. [27] investigated lead-free (Sn-3.8Ag-0.7Cu) at several temperatures from -25°C to 125°C and noted that the fatigue failure is dependent on the temperature where the fatigue life of solder decreases with increasing the temperature. By contrast, when comparing the low-cycle fatigue lives of 60Sn-40Pb at -50, 35, and 125°C, Solomon et al. [28] did not find any difference. Vaynman et al. [29] similarly found no effect on the fatigue life of bulk cast lead-tin solder specimens, including 96.5Pb-3.5Sn and 63Sn-37Pb, tested at 25°C to 80°C. Anderson et al. [30] tested both bulk and solder joint samples of lead-free solders (Sn-3.5Ag) and (Sn-4.0Ag-0.5Cu), and compared their behaviours with lead-tin eutectic (Sn-37Pb) and found that the isothermal fatigue life of lead-free solders was generally better. Solomon [31] compared the isothermal fatigue behaviour of two simple eutectic solders, Sn-3.5Ag and Sn-40Pb, at 35°C and 150°C using single lap joints and they have found that the life of Sn-3.5Ag solders was longer than that of Sn-40Pb at both temperatures.

The basic mechanical properties and fatigue lives of solders depend mainly on their microstructures and its evolution during solidification and loading. The term “microstructure” describes the morphology, grain size and configuration, and distribution of phases in a metallic system and the mechanical strength and the long term reliability of solder joints are directly dependent on the microstructure formed when the liquid solder solidifies to form a solder joint [32]. Thus, a full understanding of fatigue behaviour cannot be achieved without assessing the microstructure of the solder samples [33]. The melting temperature of Sn-37Pb solder is 182°C, which is lower than that of Sn-Ag-Cu solders. The lower melt temperature

combined with the presence of soft Pb islands in Sn3-7Pb, as opposed to hard intermetallics in Sn-Ag-Cu solder, causes higher fatigue damage in Sn-37Pb compared to the Sn-Ag-Cu solders. In general, the intermetallic compound particles possess much higher strength than the Sn matrix [34]. It has been reported that the fatigue resistance of Sn-Ag-Cu alloys is 3~4 times greater than Sn-37Pb eutectic solder. The higher fatigue resistance is ascribed to the interspersed Ag_3Sn and Cu_6Sn_5 particles, which pin and block the movement of dislocations [35].

In summary, developing reliable solder joints for the microelectronics industry requires a full understanding of their fatigue behaviour and the microstructure's evolution under different types of loadings. Although there is extensive research on the performance of solder joints under cyclic loadings, only limited investigations have conducted a comparative analysis of fatigue behaviour under different isothermal, 'in-phase' and 'out-phase' combined thermal-mechanical loadings. Thus, this paper aims to carry out a structured series of experiments linking the microstructure and thermomechanical properties of two different leaded and lead-free solders in an attempt to comprehensively understand their fatigue behaviour and associated failure mechanisms so a more reliable solder joint can be obtained.

2. Material and methods

2.1 Sample preparation

The mechanical testing was carried out on 4-ball grid array (BGA) specimens of solder joints produced using similar procedures and sizes to commercial ones. The BGA specimen is consisted of a grid of four solder balls with an approximate diameter of 0.7 mm and a pitch of 2.54 mm, as shown in Figure 1.

Printed Circuit Board (PCB) was made of glass fibre reinforced polymer (FR-4) substrate plates diced to 5 mm × 5 mm with four copper pads etched onto the plate as shown in Figure 2. The shape of copper pads is circular with a diameter of 0.7 mm and a thickness of 35 μm and plated with 5 μm of tin. The FR-4 plate is an 8-ply glass-epoxy laminate with an overall

thickness of 1.5 mm containing 40% glass fibres woven in a 0°/90° configuration. The solder was applied as a paste via a specially-designed stencil with four balls and the specimen formed by reflow soldering in a special jig. Once solder paste had been inserted into the holes it was pressed down against the copper pads with a specially-fabricated steel pin. The substrate was then removed from the jig leaving four pillars of solder paste applied to the copper surface. Both the jig and pin were cleaned with Multicor SC-01 flux before applying the solder. A polished cross-section of the FR-4 material is shown in Figure 3, where it can be seen that the fibre bundles are roughly lenticular in shape and each fibre has an approximate diameter of 7 μm.

The substrate with the solder paste pillars was placed together with another identical bare substrate (i.e. with no solder paste) in the jig as shown in

Figure **4** and the spacers slid into place. The entire assembly was then placed into a hot-air reflow oven to melt the solder paste and join the substrates together. The assemblies were first preheated from room temperature to a soak temperature and held for 90 sec, as indicated in Table 1. The peak temperature was then raised to approximately 30-40 °C above the melting point for 60 seconds. Following reflow, the specimen was pushed out of the jig by inserting a pin into a pre-drilled hole in the centre of the alignment jig. Figure 5 shows a typical assembly after reflow.

2.2 Metallography

Considering that the mechanical strength of solder joints is directly dependent on its microstructure, it was critically important to characterise the solder samples as closely as possible using microscopic examination to establish the phase structure. It is well known that the microstructure of Sn-3.8Ag-0.7Cu lead-free solders is very different from leaded solder Sn-37Pb. However, both leaded and lead-free solder alloys are very soft with low recrystallization temperatures and so they should be carefully prepared for metallographic examination. First, the solder alloys samples were mounted into resin at room temperature. Thereafter grinding and polishing were performed using a universal polishing machine.

Specimens were wet ground using 240, 600, 800, 1000, 1200, and 4000 grit silicon carbide papers in sequence with water as the lubricant with about 5 minutes per step. The specimens and the paper were cleaned between each grinding step to remove loose particles of abrasive and specimens were manipulated carefully to minimise the probability that abrasive particles could become embedded in the solder. Specimens were polished using a similar grinding technique, again serially using 9 μm, 1 μm and 0.5 μm diamond paste on a canvas cloth. Next, 0.5 μm alumina suspension was used to remove any scratch marks, followed by a final finish using colloidal silica polish on a micro cloth. Samples were examined under an optical microscope between polishing steps and stages were repeated if necessary. For optical microscope and scanning electron microscope (SEM) metallography, samples had to be only lightly etched and had to be examined when fresh. The leaded solder samples had sufficient contrast in the as-polished state and were therefore not etched. For lead-free solder alloys, the etching was accomplished primarily using a dilute solution of 2% concentrated (HCL), 6% concentrated HNO_3 and 92 % H_2O for about 3 seconds because this is often strong enough to reveal the microstructure of Sn-3.8Ag-0.7Cu.

The prepared samples were imaged using optical microscope and scanning electron microscope (SEM) to study the metallography.

2.3 Fatigue experimental apparatus

A test rig was designed to load the BGA specimens in shear as this is the most common loading direction both in service and in other studies. The test rig, as shown in Figure 6, is consisted of three distinct interconnected units to measure and control each of temperature, displacement (strain), and force (stress). The testing system is used to carry out TMF tests at a range of temperatures from ambient to 75ºC, with and without temperature cycling, under an applied shear load range. The BGA sample was fitted in a metallic heat sink and held in its place with a thin layer of a thermally conducting adhesive (WLK 30) of approximate thickness 0.15 mm. The sample was therefore loaded along the edge of the square piece of PCB, which in turn transferred the load to the solder bumps. For applying the mechanical

loading, a linear stepper motor (actuator) was used to apply the shear displacement on the top substrate while a Linear Variable Differential Transformer (LVDT) and a load cell were employed to measure the shear displacement and the reaction force, respectively. The mechanical tests were conducted in closed-loop force control using the linear stepper motor actuator (42DBL10 Series Mclennan) which provided the shear displacement. The shear displacement was increased with the load cell measuring the reaction force used for control of the actuator. The stepper motor was capable of linear displacements in the forward or backward directions in steps of 12.7 μm (a half step), with a maximum deliverable force of 100 N. A compression spring (stiffness of 25.36 kN⁄m) was used to "soften" the system, allowing longer displacements for a given force to improve the resolution of the displacement control. A LabView programme was devised to deliver the required stepper motor control signals via control board. The data acquisition interfacing card data acquisition system was based on an in-house built desktop PC with a 12 bit, National Instruments (NI), PCI-6024 data acquisition interfacing card. This card is a multifunction analogue, digital and timing device without on-board switches or jumpers so that it can be configured and calibrated by software. This card was used to collect the data as well as providing the feedback control signal to the linear stepper motor actuator.

For applying the thermal loading, Peltier device (37.9 W and 3.9A), which is sandwiched between two heat sinks, as shown in Figure 6, was used for heating the specimen. The temperature control was achieved using a thermocouple, a temperature controller, and a data acquisition unit (DAQ) connected to a PC. The thermocouple was placed between the two substrates and was used to measure the temperature and to provide closed-loop feedback for controlling the Peltier device in isothermal and thermal cycling tests. The temperature control system was combined with the aforementioned closed-loop feedback control system of the linear stepper motor actuator via the NI 6024 card to allow measuring and control the force, displacement, and temperature in real time.

Mechanical testing of solder materials at a realistic scale involves measuring very small displacements at relatively high loads. Also, the inclusion of temperature cycling requires careful calibration to ensure that the expansion and contraction of the rig do not interfere with the strain measurement. Therefore, all the sensors used in this experimental rig, i.e. load cell, LVDT, and thermocouple, were calibrated carefully and all proved to be linear within their working range.

3. Experimental results

3.1 Microstructure characterisation

Figure 7 shows representative back-scattered scanning electron micrographs of the un-etched leaded solder. The structure consists of a relatively homogeneous distribution of the lead-rich phase (light areas) in a darker matrix of the tin-rich phase.

Figure 8-10 show a selection of optical and SEM micrographs in both unetched and etched conditions to give an overview of the microstructure of the lead-free solder. As it can be seen, the microstructure of Sn-3.8Ag-0.7Cu consists mainly of a mixture of precipitate-free β-Sn dendrites and between whose arms there is a very fine interdendritic eutectic (a mixture of Sn, Ag_3Sn and Cu_6Sn_5). Another feature of the microstructure is the presence of relatively large, isolated primary Ag_3Sn, Cu6Sn5 particles, the Ag_3Sn assuming an acicular (needle) shape and the Cu_6Sn_5 taking a more disc-like morphology with distinctive hexagonal boundaries.

These micrographs together illustrate the fundamentally different nature of the microstructure of the lead-free alloy compared to the leaded solder. The microstructure of Sn-37Pb is more homogeneous than that of Sn-3.8Ag-0.7Cu. Although both solders are fundamentally eutectics with a β-Sn dendritic matrix, the primary dendrites are much more pronounced in the lead-free alloy. Also, despite that the intermetallic compounds (IMCs) constitute only a small fraction of the final microstructure, they have a much greater effect on the mechanical strength [36]. However, this also means that the strength will be critically dependent on the

amount, size and distribution of the IMCs because very large particles will introduce brittle paths into the solder increasing the chance of local or global brittle fractures.

3.2 Stress-life behaviour

Four main groups of fatigue tests, including one with isothermal mechanical cyclic loading and three with combined thermal-mechanical cyclic loading, were conducted to investigate the reliability of both solder alloys. For the combined loading tests, the mechanical and thermal cycles were either at the same frequency and in-phase (IP), or at the same frequency but out-of-phase (OoP), or at a different frequency (nIP). All tests were conducted under load-control settings. Stress-life results based on the number of the cycles to failure were obtained at different stress amplitudes levels for each type of the tests, i.e. isothermal, IP, OoP, and nIP. In each case, the nominal shear stress range was calculated by dividing the force by the total nominal cross-sectional area of the solder balls. Standard stress-number of cycles (S-N) curves are plotted on log-log axes for the stress range against the number of cycles to failure. The best fit lines of the fatigue lives data were also obtained for each type of the tests. The general equation of the best-fit line of stress range as a function of the number of cycles in log-log format is shown in Eq (1)

$$log\ S = \log S1 + m \log N \qquad \text{Eq (1)}$$

Where S is the stress range, N is the number of cycles, S1 and m are the fit line constants.

Tests were terminated at 10^5 cycles if the assembly had not failed and were classed as run-outs. The run-out tests were repeated twice to ensure the repeatability of the obtained results. All the obtained results showed good trend at the at the different stress levels. Table 2 summarises the systematic tests.

3.2.1 IF behaviour

Figure 11 presents S-N curves for the isothermal mechanical fatigue tests of leaded and lead-free solder alloys at the three different temperatures including RT (25°C), 35°C and 75°C.

As can be seen, all the curves show the broadly expected shape of decreasing life with increasing stress range. Additionally, the fatigue lives of both solder alloys decrease with increasing the temperature. Also, the lead-free alloy exhibits a consistently longer fatigue life than those made with leaded solder and this difference increases as the temperature increases. Finally, the difference between leaded and lead-free assembly performance tends to decrease as the stress range increases, except at the highest temperature where it remains about the same over the range studied.

3.2.2 nIP TMF behaviour

In these tests, the temperature and shear stress were not cycled at the same frequency and thus they can be considered as neither in-phase nor out-of-phase (nIP) combined cycling loadings. The temperature of the thermal loading was cycled between 35**°C** and 75**°C** with a lower frequency than that of the mechanical loading. These tests were included to assess if there is an inherent effect of temperature cycling over and above that which is associated with the thermal strain, so a reduced set of stress-life tests were repeated at the same frequency, but with a superimposed lower frequency temperature.

Since the thermal and mechanical cycles are neither in-phase nor out-of-phase, if there were no additional effect, the samples might be expected to behave as isothermal tests with a mean temperature of 55°C. Figure 12 summarises the lifetime behaviour under nIP temperature-stress cycling. It is clear that the nIP behaviour of lead-free solder is better than that of leaded solder. Comparing Figure 12 with Figure 11, it can be seen that nIP curves lie roughly mid-way between the 35°C and 75°C isothermal curves.

3.2.3 IP and OoP TMF behaviour

These tests were conducted under variable temperature ranged from 30 °C to 80°C but at the same of frequency of stress cycle.

Figure 13 summarises the lifetime behaviour of Sn-3.8Ag-0.7Cu and Sn-37Pb under IP and OoP loadings. It can easily be observed that the fatigue life of Sn-3.8Ag-0.7Cu is better than

Sn-37Pb under both types of temperature-stress cycling loads, i.e. IP and OoP. Surprisingly, OoP lives seems to be somewhat counter-intuitive as OoP loading results in shorter fatigue life than IP loading for both types of solders. Such behaviour is most pronounced in Sn-3.8Ag-0.7Cu at high stress range and least pronounced for Sn-37Pb at high stress range. The effect is more-or-less constant for the leaded solder at all stress ranges studied.

4. Discussion

Figure 14 compares the S-N curves for all tests conducted in this study. Table 3 presents the constants of best fit line for all S-N curves. The S-N curves of Sn-3.8Ag-0.7Cu behave in a broadly similar fashion to those of Sn-37Pb alloy. The main difference is that the scatter on the lines is greater and the curves are less consistently parallel for Sn-3.8Ag-0.7Cu. Such trend could be due to the greater microscopic heterogeneity and inhomogeneity microstructure of Sn-3.8Ag-0.7Cu compared to Sn-37Pb. As it can be seen Figure 14 from and Table 3, the IF lives of both solders decrease in an approximately exponential fashion with temperature throughout the range. Sn-3.8Ag-0.7Cu solder is more resistant to isothermal fatigue than Sn-37Pb solder and exhibit longer IF lives at both room and elevated temperatures. These observations are consistent with those reported in literature. Korhonen et al. [27] studied isothermal mechanical fatigue resistance of Sn-3.8Ag-0.7Cu and reported that its durability was decreased with increasing the temperature. Andersson et al. [30] and Wiese et al. [15] found that the fatigue life of lead-free solders including Sn-3.5Ag, Sn-4.0Ag-0.5Cu, and Sn-4Ag-0.5Cu, was better than Sn-37Pb at room temperature. Other alloys using intermetallic compound (IMC) particle hardening, such as Sn-8Zn-3Bi have also been found to have longer fatigue life than Sn-37Pb at room temperature [22,23]. Solomon et al. [31] found that the IF resistance of both eutectic Sn-Ag and Sn-40Pb single lap joints decrease with increasing the temperature and the fatigue life of lead-free solder joints to be longer than that of leaded solder joints at both 35°C and 150°C. Zhang et al. [19] studied three levels of IMC strengthening including Sn-3.9Ag-0.6Cu, Sn-3.5Ag, and Sn-0.7Cu and found that the

fatigue resistance of all three lead-free solder alloys was better than Sn-37Pb at elevated temperatures.

In order to understand the mechanism associated with the fatigue failure under isothermal conditions, the IF tests were used to created Arrhenius plots and to estimate the activation energies for both leaded and unleaded solder alloys. Figure 15 shows an Arrhenius plot of the time to failure at a fixed stress for each of the isothermal tests (including nIP). The slop of this curve (Q/R) represents the activation energy which is equal to $4000K^{-1}$ for Sn-37Pb. Jung et al. [37] measured an activation energy of $4800K^{-1}$ for microstructural coarsening during static annealing of 60Sn-40Pb. Additionally, Vianco et al. [38] have found that the activation energy for microstructural coarsening of 60Sn-40Pb ranging between 1900 and $4900K^{-1}$ depending on the starting microstructure where the finer microstructures were found to have higher activation energies. It therefore seems that the same processes as govern particle coarsening (in this case, diffusion of lead in solid tin) are influencing the susceptibility to isothermal fatigue (including the nIP tests). The coarsened grains of Sn-Pb are inherently weak and constitute the medium for cracks initiation and propagating leading to complete solder failure.

Arrhenius plot of Sn-3.8Ag-0.7Cu was also created as shown in Figure 16. Based on this plot, the activation energy was calculated as 5185 K^{-1} which is higher than that one of Sn-Pb indicating a longer fatigue life. This variation probably reflects the more complex microstructural changes going on Sn-3.8Ag-0.7Cu, where two phases including Cu_6Sn_5 and Ag_3Sn are involved, with two distinct size distributions as primary and eutectic particles, respectively. Dutta et al. [39] suggested that the coarsening of Ag_3Sn is related to diffusion and solubility of Ag in Sn as well as the applied stress. Li et al. [40] have measured an activation energy of around $1000K^{-1}$ for Cu_6Sn_5 growth at Sn-Ag-Cu/Cu interfaces, whereas Tian et al. [41] estimated it to be around $8000K^{-1}$ for $(Cu,Ni)_6Sn_5$ and Cu_3Sn for the same alloy on Ni-plated Cu pads. This range of values, coupled with the multiple heterogeneity of

the microstructure indicate that the IF life of SAC alloy is also activated in the same way as the microstructural coarsening.

For TMF tests, i.e. IP and OoP tests, the situation appears to be more complicated, since the fatigue life in both of these conditions is considerably shorter (about a factor of 5 for the IP and a factor of 10 for the OoP) than the extrapolated nIP curve. The fatigue life is considerably shorter than even the extrapolation of the IF test at 75°C, so the effect, for the IP tests, still cannot be explained by the maximum stress always coinciding with the maximum temperature. Furthermore, such an explanation would still not account for the fatigue life being shorter for the OoP than the IP tests. Eckert et al. [42,43] studied the fatigue behaviour of solder joints under combined thermal cycling and vibration loading. They have observed that there was a clear interaction effect as the time to failure of BGA solder under combined loading was significantly shorter than that under temperature cycling or vibration alone at room temperature. The TMF lives observed here certainly seem to suggest an interaction effect between the thermal and mechanical loadings since lives are considerably shorter than an extrapolation of the equivalent isothermal curve (75ºC) would suggest.

5. Conclusion

In this paper, the reliability of leaded and lead-free solder alloys is investigated using fatigue testing rig under a wide range of loading conditions. In addition to isothermal mechanical fatigue tests, thermal-mechanical set of fatigue tests was carried out where temperature and stress cycles were either ‘in-phase’, ‘out-of-phase’, or ‘not-in-phase’. The main aim of the study was to compare the fatigue behaviour of the solders under different loading conditions and to understand the link between the microstructural evolution and fatigue performance.

Based on fatigue life measurements in solder joints, it was observed that the Sn-3.8Ag-0.7Cu alloy showed better fatigue performance than Sn-37Pb under all conditions tested, although its S-N curves exhibited greater scatter. Additionally, the lead-free solder was more resistant to degradation in durability as the temperature increases and exhibited higher activation

energy than the leaded solder. The microstructural coarsening of both alloys was found to be the main mechanism dominating the isothermal fatigue behaviour.

The thermal-mechanical fatigue lives were generally shorter than would be expected when extrapolating from the corresponding isothermal fatigue range. Such behaviour suggests interaction effects resulting from the combined thermal and mechanical cyclic loadings.

Acknowledgement

The authors would like to acknowledge the kind advice and assistance of Dr Hector Steen of Henkel Ltd. for the provision of solder paste and invaluable technical advice.

References

[1] J. Thambi, U. Tetzlaff, A. Schiessl, K.D. Lang, M. Waltz, Evaluation of the relationship between stress and lifetime of Pb-free solder joints subjected to vibration load using a generalized local stress approach, Microelectron. Reliab. 106 (2020) 113560. doi:10.1016/j.microrel.2019.113560.

[2] H. Wang, K. Pan, J. Ha, C. Cai, J. Xu, S. Park, The effect of solder paste volume on chip resistor solder joint fatigue life, in: Procedia Manuf., Elsevier B.V., 2019: pp. 1372–1380. doi:10.1016/j.promfg.2020.01.151.

[3] T.T. Dele-Afolabi, M.A.A. Hanim, R. Calin, R.A. Ilyas, Microstructure evolution and hardness of MWCNT-reinforced Sn-5Sb/Cu composite solder joints under different thermal aging conditions, Microelectron. Reliab. 110 (2020) 113681. doi:10.1016/j.microrel.2020.113681.

[4] I.C. Wu, M.H. Wang, L.S. Jang, Experimental location of damage in microelectronic solder joints after a board level reliability evaluation, Eng. Fail. Anal. 83 (2018) 131–140. doi:10.1016/j.engfailanal.2017.10.002.

[5] K.C. Otiaba, R.S. Bhatti, N.N. Ekere, S. Mallik, M. Ekpu, Finite element analysis of the effect of silver content for Sn-Ag-Cu alloy compositions on thermal cycling reliability of solder die attach, Eng. Fail. Anal. 28 (2013) 192–207.

doi:10.1016/j.engfailanal.2012.10.008.

[6] J. Jiao, X. De, Z. Chen, T. Zhao, Integrated circuit failure analysis and reliability prediction based on physics of failure, Eng. Fail. Anal. 104 (2019) 714–726. doi:10.1016/j.engfailanal.2019.05.021.

[7] Proposal for a Directive of the European Parliament and of the Council on waste electrical and electronic equipment (WEEE), (n.d.). https://eur-lex.europa.eu/legal-content/EN/ALL/?uri=CELEX:52008PC0810 (accessed June 26, 2020).

[8] M.N. Collins, E. Dalton, J. Punch, Microstructural influences on thermomechanical fatigue behaviour of third generation high Ag content Pb-Free solder alloys, J. Alloys Compd. 688 (2016) 164–170. doi:10.1016/j.jallcom.2016.07.191.

[9] C. Kanchanomai, Y. Mutoh, Temperature effect on low cycle fatigue behavior of Sn{\textendash}Pb eutectic solder, Scr. Mater. 50 (2004) 83–88. doi:10.1016/j.scriptamat.2003.09.034.

[10] S. Vaynman, Fatigue life prediction of solder material: effect of ramp time, hold time and temperature, in: 40th Conf. Proc. Electron. Components Technol., IEEE, n.d. doi:10.1109/ectc.1990.122235.

[11] B. Hu, P. Zhou, J. Zhou, Y. Yang, F. Wan, The Effect of Temperature on Low Cycle Fatigue of an Eutectic Solder, in: 2006 Int. Conf. Electron. Mater. Packag., IEEE, 2006. doi:10.1109/emap.2006.4430694.

[12] C. Kanchanomai, Y. Mutoh, Low-cycle fatigue prediction model for pb-free solder 96.5Sn-3.5Ag, J. Electron. Mater. 33 (2004) 329–333. doi:10.1007/s11664-004-0139-1.

[13] J. Pang, Low cycle fatigue study of lead free 99.3Sn{\textendash}0.7Cu solder alloy, Int. J. Fatigue. 26 (2004) 865–872. doi:10.1016/j.ijfatigue.2003.12.004.

[14] Y. Kariya, M. Otsuka, Mechanical fatigue characteristics of Sn-3.5Ag-X (X=Bi, Cu, Zn and In) solder alloys, J. Electron. Mater. 27 (1998) 1229–1235. doi:10.1007/s11664-998-0074-7.

[15] S. Wiese, S. Jakschik, F. Feustel, E. Meusel, Fracture behaviour of flip chip solder

joints, in: 2001 Proceedings. 51st Electron. Components Technol. Conf. (Cat. No.01CH37220), IEEE, n.d. doi:10.1109/ectc.2001.927998.

[16] T.-S. Park, S.-B. Lee, Low Cycle Fatigue Testing of Ball Grid Array Solder Joints under Mixed-Mode Loading Conditions, J. Electron. Packag. 127 (2004) 237–244. doi:10.1115/1.1871192.

[17] T.-S. Park, S.-B. Lee, Cyclic stress-strain measurement tests of Sn3.5Ag0.75Cu solder joint, in: Proc. 4th Int. Symp. Electron. Mater. Packag. 2002., IEEE, n.d. doi:10.1109/emap.2002.1188858.

[18] K.O. Lee, J. Yu, T.S. Park, S.B. Lee, Low-cycle fatigue characteristics of Sn-based solder joints, J. Electron. Mater. 33 (2004) 249–257. doi:10.1007/s11664-004-0130-x.

[19] Q. Zhang, A. Dasgupta, P. Haswell, Isothermal Mechanical Durability of Three Selected {PB}-Free Solders: Sn3.9Ag0.6Cu, Sn3.5Ag, and Sn0.7Cu, J. Electron. Packag. 127 (2005) 512–522. doi:10.1115/1.2056569.

[20] G. Cuddalorepatta, A. Dasgupta, Effect of cyclic fatigue damage accumulation on the elastic-plastic properties of SAC305 solders, in: 2009 10th Int. Conf. Therm. Mech. Multi-Physics Simul. Exp. Microelectron. Microsystems, EuroSimE 2009, 2009. doi:10.1109/ESIME.2009.4938503.

[21] Y. Kanda, Y. Kariya, Influence of Asymmetrical Waveform on Low-Cycle Fatigue Life of Micro Solder Joint, J. Electron. Mater. 39 (2009) 238–245. doi:10.1007/s11664-009-1003-0.

[22] P. Sun, C. Andersson, X. Wei, Z. Cheng, D. Shangguan, J. Liu, Coffin-Manson constant determination for a Sn-8Zn-3Bi lead-free solder joint, Solder. Surf. Mt. Technol. 18 (2006) 4–11. doi:10.1108/09540910610665071.

[23] P. Sun, C. Andersson, Z. Cheng, Z. Lai, D. Shangguan, J. Liu, Coffin-Manson Equation determination for Sn-Zn Based Lead-Free Solder Joints, in: 2005 Conf. High Density Microsyst. Des. Packag. Compon. Fail. Anal., IEEE, 2005. doi:10.1109/hdp.2005.251421.

[24] M. Dusek, C. Hunt, Low Cycle Isothermal Fatigue Properties of Lead-free Solders, in:

2007 9th Electron. Packag. Technol. Conf., IEEE, 2007. doi:10.1109/eptc.2007.4469837.

[25] D. Di Maio, C. Murdoch, O. Thomas, C. Hunt, The degradation of solder joints under high current density and low-cycle fatigue, in: 2010 11th Int. Therm. Mech. Multi-Physics Simulation, Exp. Microelectron. Microsystems, IEEE, 2010. doi:10.1109/esime.2010.5464601.

[26] C. Kanchanomai, Y. Mutoh, Effect of temperature on isothermal low cycle fatigue properties of Sn{\textendash}Ag eutectic solder, Mater. Sci. Eng. A. 381 (2004) 113–120. doi:10.1016/j.msea.2004.04.018.

[27] T.-M.K. Korhonen, L.P. Lehman, M.A. Korhonen, D.W. Henderson, Isothermal Fatigue Behavior of the Near-Eutectic Sn-Ag-Cu Alloy between -25{\textdegree}C and 125{\textdegree}C, J. Electron. Mater. 36 (2007) 173–178. doi:10.1007/s11664-006-0048-6.

[28] H. Solomon, Fatigue of 60/40 Solder, {IEEE} Trans. Components, Hybrids, Manuf. Technol. 9 (1986) 423–432. doi:10.1109/tchmt.1986.1136672.

[29] S. Vaynman, Effect of temperature on isothermal fatigue of solders, {IEEE} Trans. Components, Hybrids, Manuf. Technol. 13 (1990) 909–913. doi:10.1109/33.62555.

[30] C. Andersson, Z. Lai, J. Liu, H. Jiang, Y. Yu, Comparison of isothermal mechanical fatigue properties of lead-free solder joints and bulk solders, Mater. Sci. Eng. A. 394 (2005) 20–27. doi:10.1016/j.msea.2004.10.043.

[31] H.D. Solomon, Low Cycle Fatigue of Sn96 Solder With Reference to Eutectic Solder and a High Pb Solder, J. Electron. Packag. 113 (1991) 102–108. doi:10.1115/1.2905374.

[32] M.A. Matin, W.P. Vellinga, M.G.D. Geers, Microstructure evolution in a Pb-free solder alloy during mechanical fatigue, Mater. Sci. Eng. A. 431 (2006) 166–174. doi:10.1016/j.msea.2006.05.144.

[33] A. Boulaajaj, J.M. Cabrera, J.M. Prado, Effect of initial microstructure, frequency and temperature on the low cycle fatigue behaviour of the soldering alloys 96.5Sn-3.5Ag

and 63Sn-37Pb, Eng. Fail. Anal. 15 (2008) 220–228. doi:10.1016/j.engfailanal.2007.06.001.

[34] R. Sayyadi, H. Naffakh-Moosavy, The Role of Intermetallic Compounds in Controlling the Microstructural, Physical and Mechanical Properties of Cu-[Sn-Ag-Cu-Bi]-Cu Solder Joints, Sci. Rep. 9 (2019). doi:10.1038/s41598-019-44758-3.

[35] S. Ganesan, J.S. Xie, H. Qi, M. Osterman, Review of Lead-free Solder Joint Reliability, in: Lead-Free Electron., John Wiley & Sons, Inc., 2006: pp. 139–235. doi:10.1002/047000780x.ch5.

[36] L. Snugovsky, P. Snugovsky, D.D. Perovic, T. Sack, J.W. Rutter, Some aspects of nucleation and growth in Pb free Sn{\textendash}Ag{\textendash}Cu solder, Mater. Sci. Technol. 21 (2005) 53–60. doi:10.1179/174328405x13994.

[37] K. Jung, H. Conrad, Microstructure coarsening during static annealing of 60Sn40Pb solder joints: {II} eutectic coarsening kinetics, J. Electron. Mater. 30 (2001) 1303–1307. doi:10.1007/s11664-001-0115-y.

[38] P. Vianco, J. Rejent, G. Zender, A. Kilgo, Kinetics of Pb-rich Phase Particle Coarsening in Sn{\textendash}Pb Solder Under Isothermal Annealing{\textendash}cooling Rate Dependence, J. Mater. Res. 20 (2005) 1563–1573. doi:10.1557/jmr.2005.0198.

[39] I. Dutta, D. Pan, R.A. Marks, S.G. Jadhav, Effect of thermo-mechanically induced microstructural coarsening on the evolution of creep response of {SnAg}-based microelectronic solders, Mater. Sci. Eng. A. 410–411 (2005) 48–52. doi:10.1016/j.msea.2005.08.142.

[40] X. Li, F. Li, F. Guo, Y. Shi, Effect of Isothermal Aging and Thermal Cycling on Interfacial {IMC} Growth and Fracture Behavior of {SnAgCu}/Cu Joints, J. Electron. Mater. 40 (2010) 51–61. doi:10.1007/s11664-010-1401-3.

[41] Y. Tian, J. Chow, X. Liu, Y.P. Wu, S.K. Sitaraman, Study of Intermetallic Growth and Kinetics in Fine-Pitch Lead-Free Solder Bumps for Next-Generation Flip-Chip Assemblies, J. Electron. Mater. 42 (2012) 230–239. doi:10.1007/s11664-012-2302-4.

[42] T. Eckert, M. Kruger, W.H. Muller, N.F. Nissen, H. Reichl, Investigation of the solder joint fatigue life in combined vibration and thermal cycling tests, in: 2010 Proc. 60th Electron. Components Technol. Conf., IEEE, 2010. doi:10.1109/ectc.2010.5490854.

[43] T. Eckert, W.H. Muller, N.F. Nissen, H. Reichl, Modeling solder joint fatigue in combined environmental reliability tests with concurrent vibration and thermal cycling, in: 2009 11th Electron. Packag. Technol. Conf., IEEE, 2009. doi:10.1109/eptc.2009.5416456.

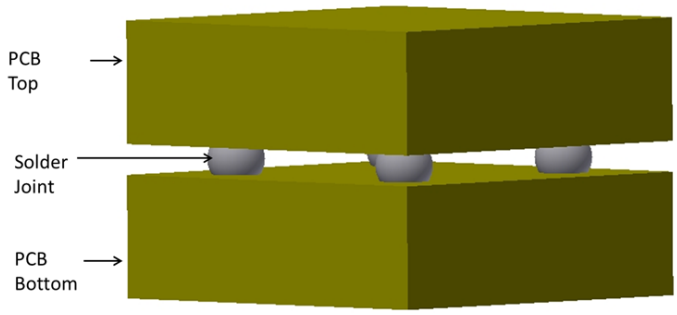

Figure 1: Schematic design of the solder joint specimen

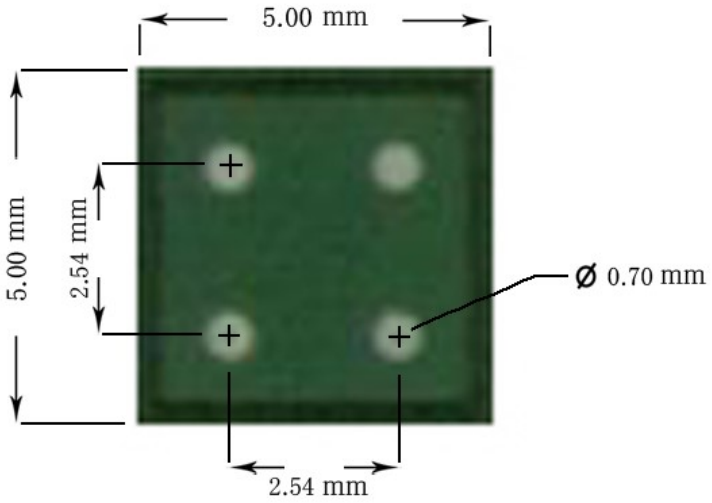

Figure 2: Typical FR-4 substrate after dicing

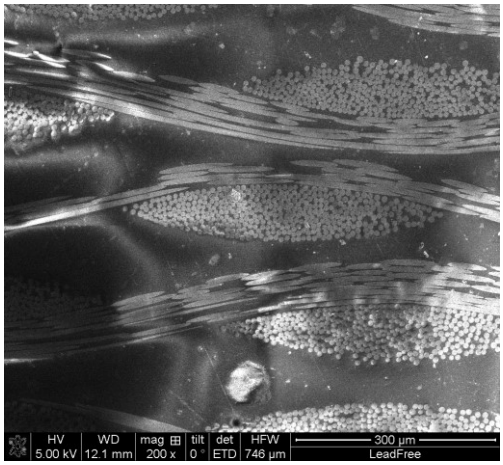

Figure 3: SEM image of cross section of FR-4 substrate

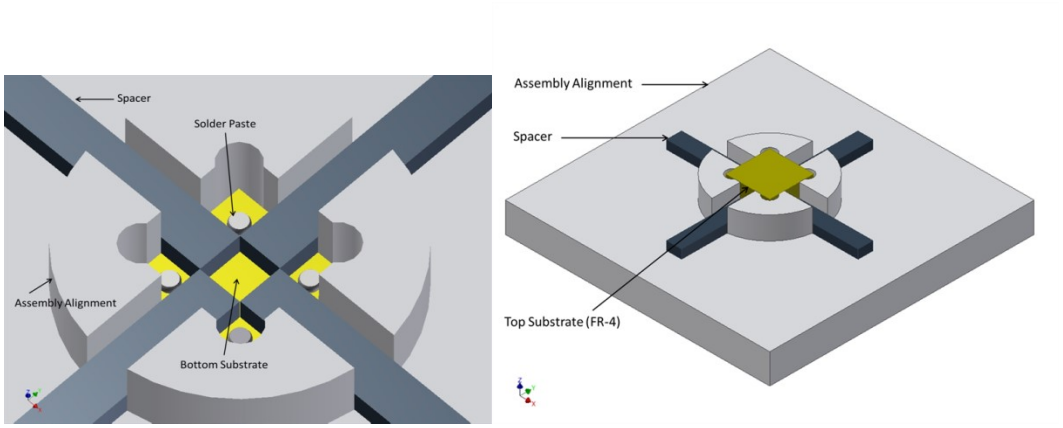

Figure 4: The entire assembly with spacer: right diagram shows bottom substrate view, left diagram show top substrate view

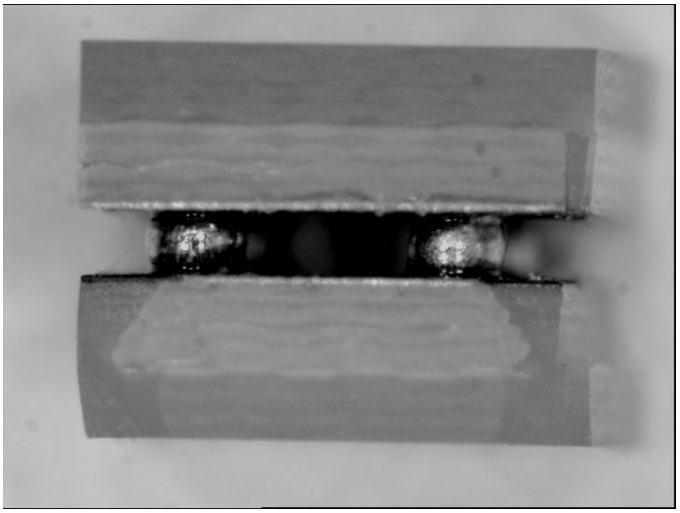

Figure 5: Typical 4-ball BGA specimen

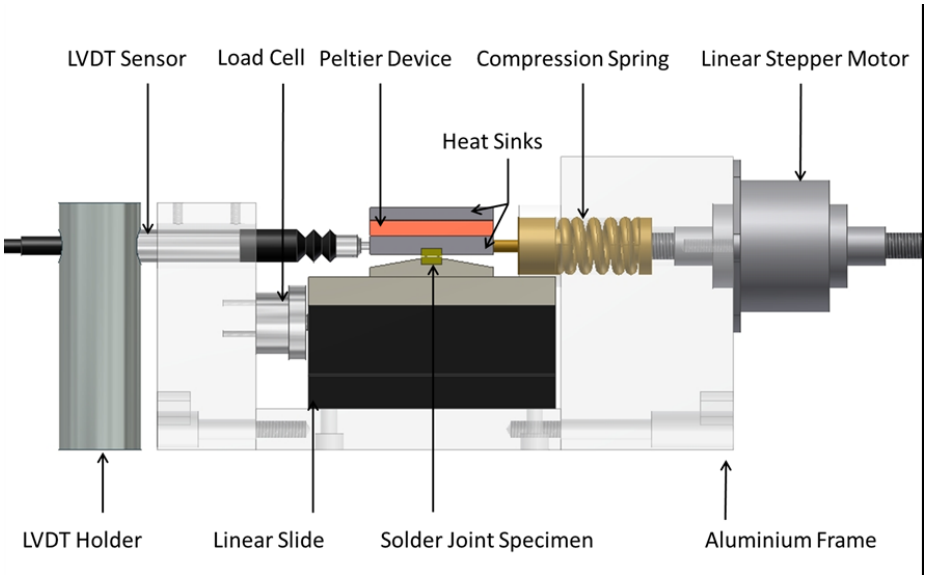

(a)

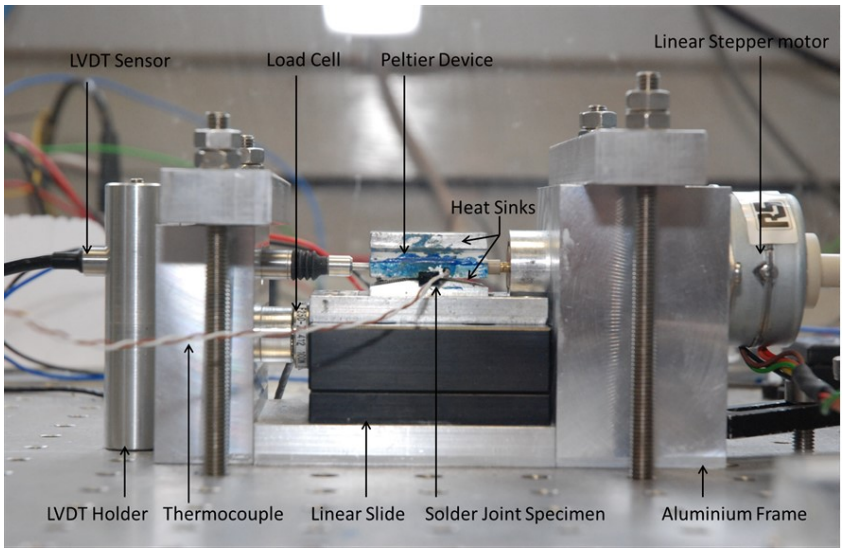

(b)

Figure 6: (a) Diagrammatic illustration of experimental setup (b) Photograph of the actual experimental rig

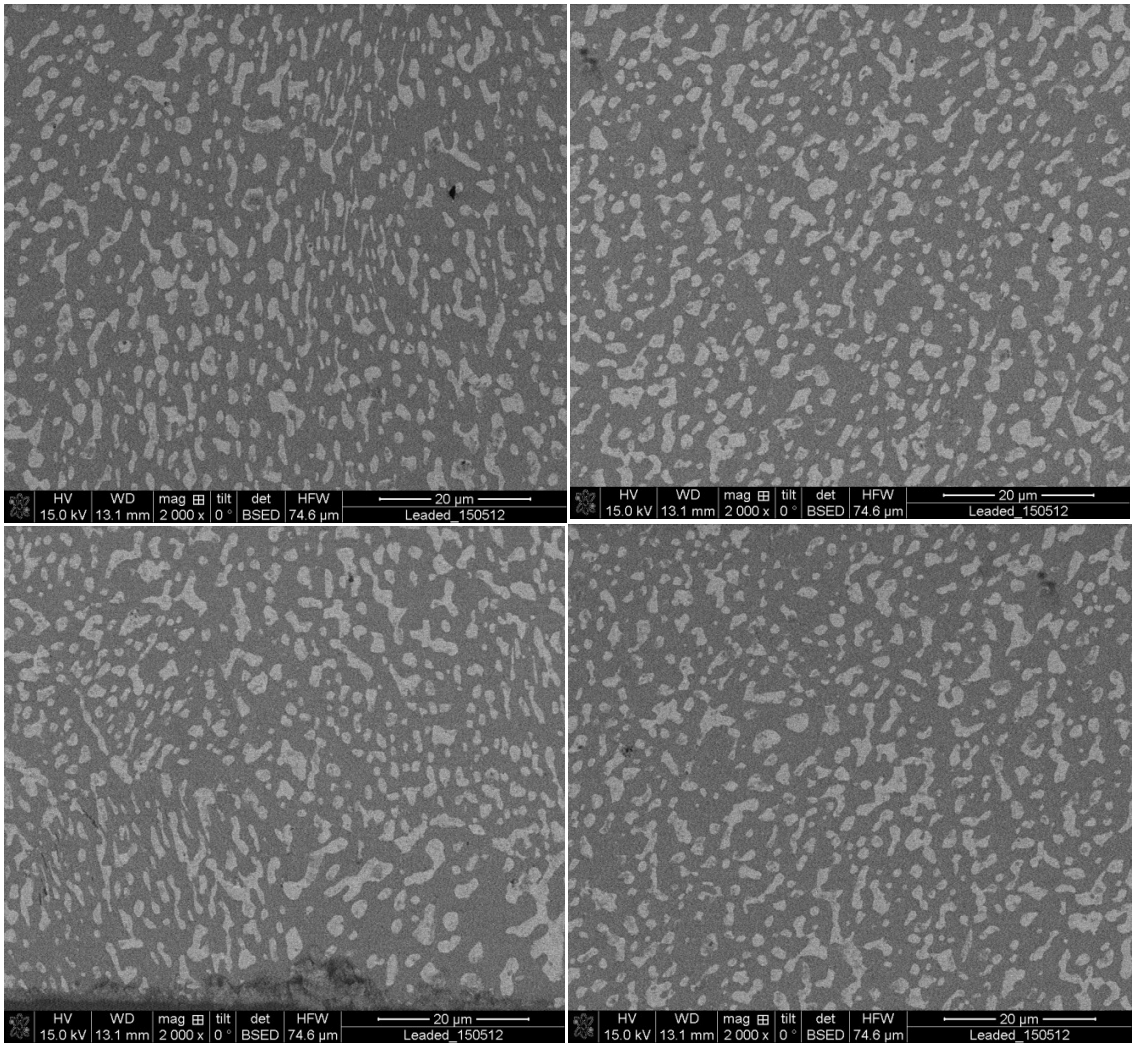

Figure 7: Back-scatter SEM images of eutectic (Sn-37Pb) solder

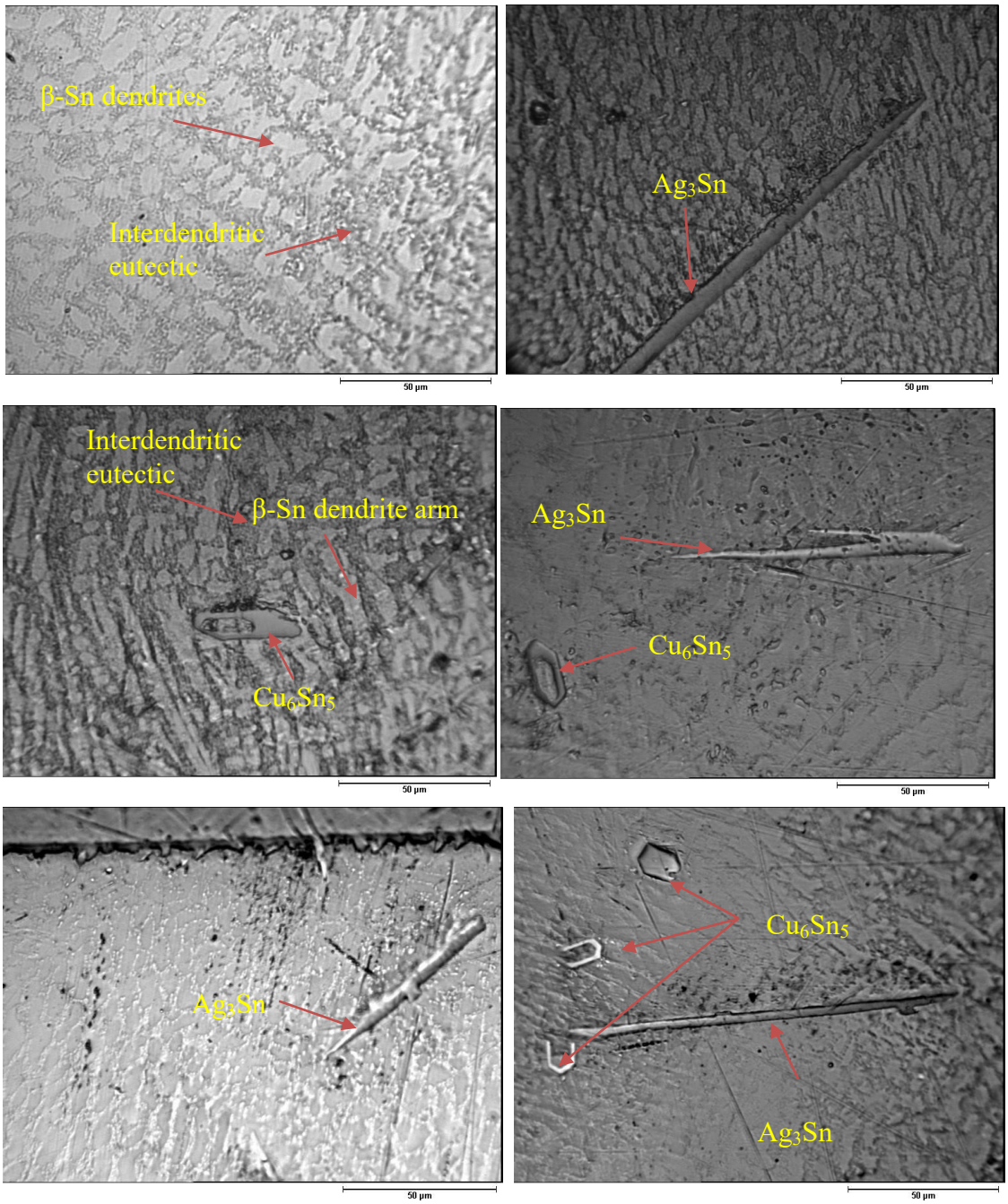

Figure 8: Optical microstructure of un-etched lead-free solder

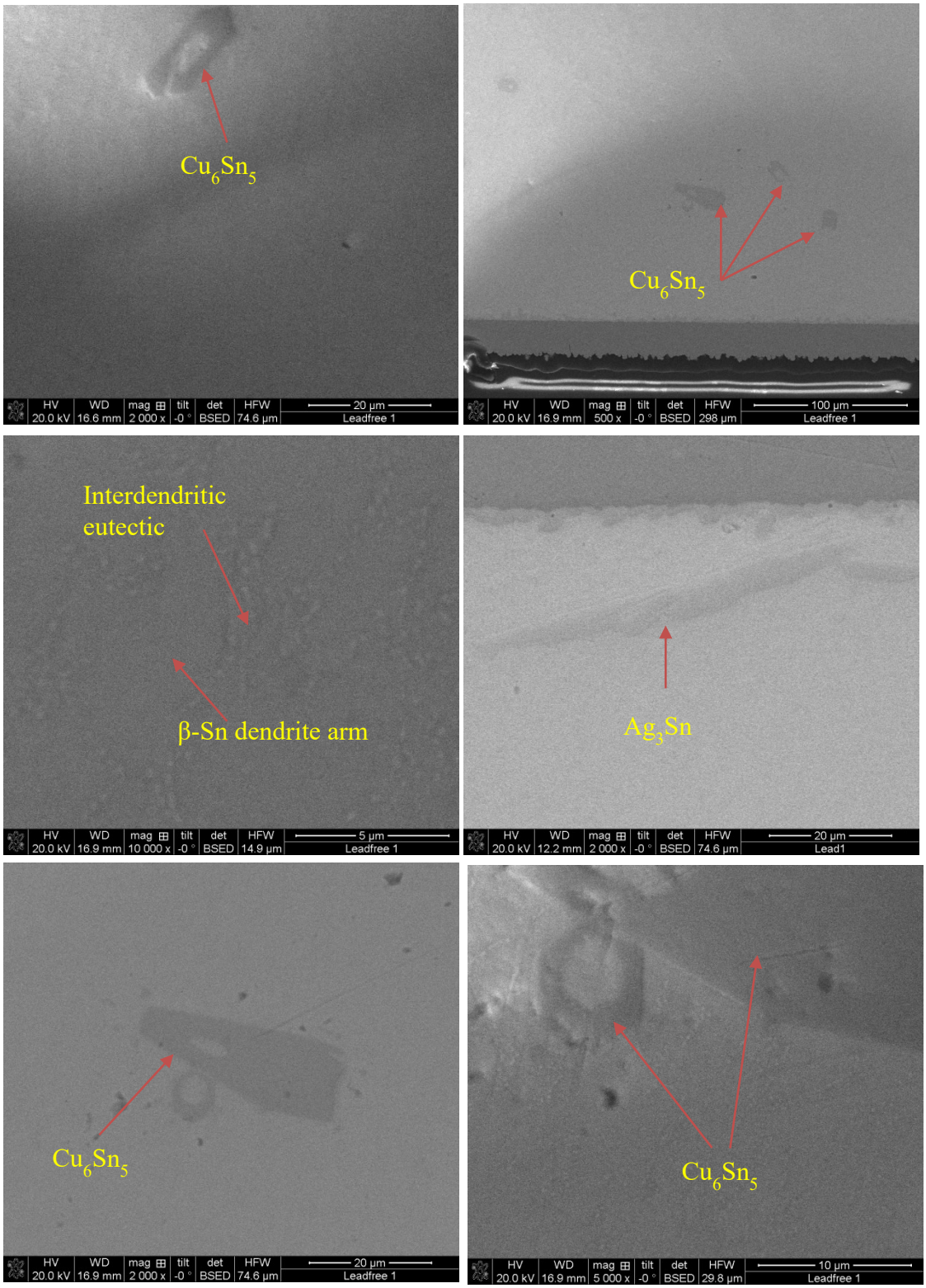

Figure 9: SEM microstructure of un-etched lead-free solder

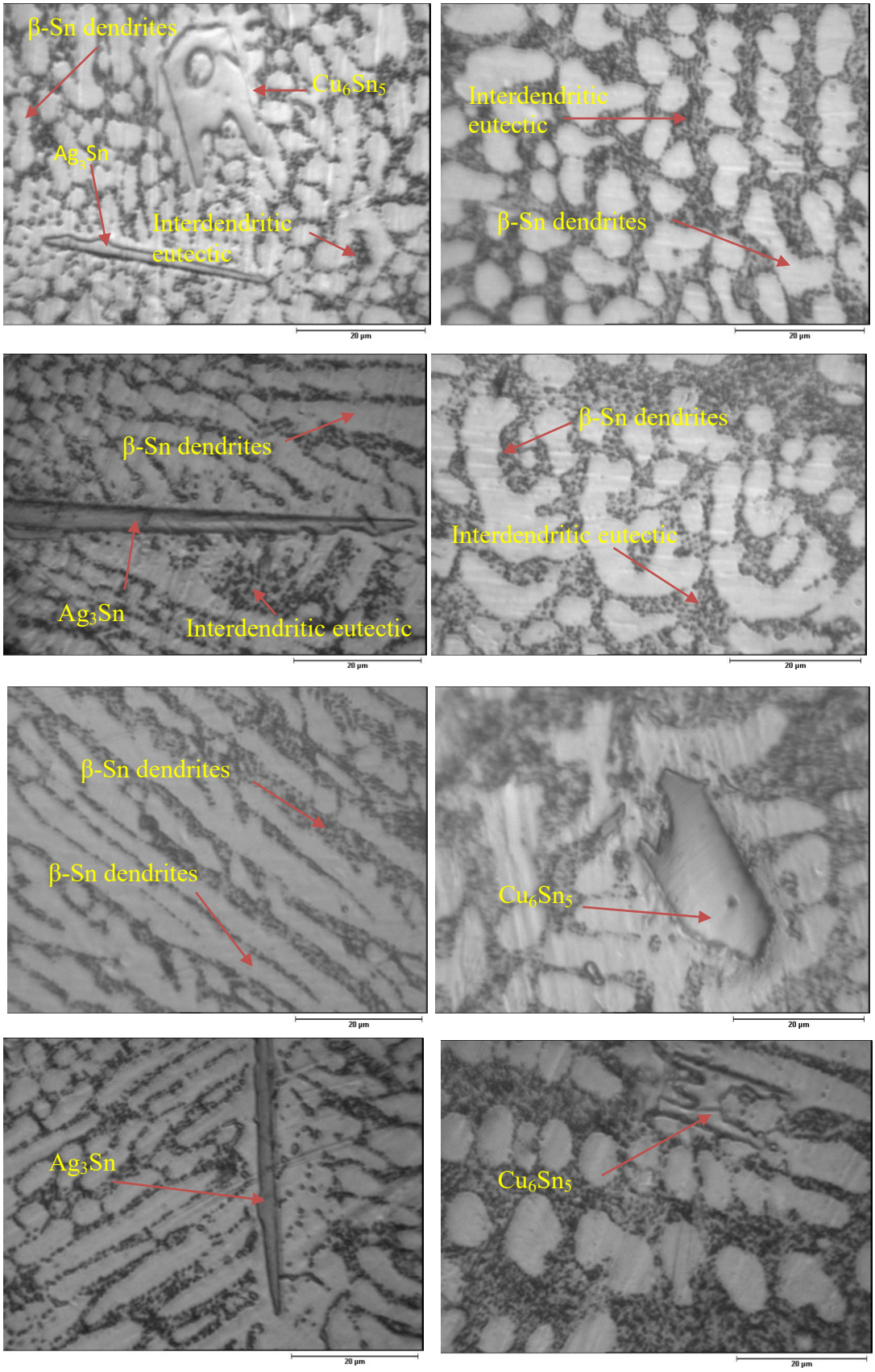

Figure 10: Optical microstructure of etched lead-free solder

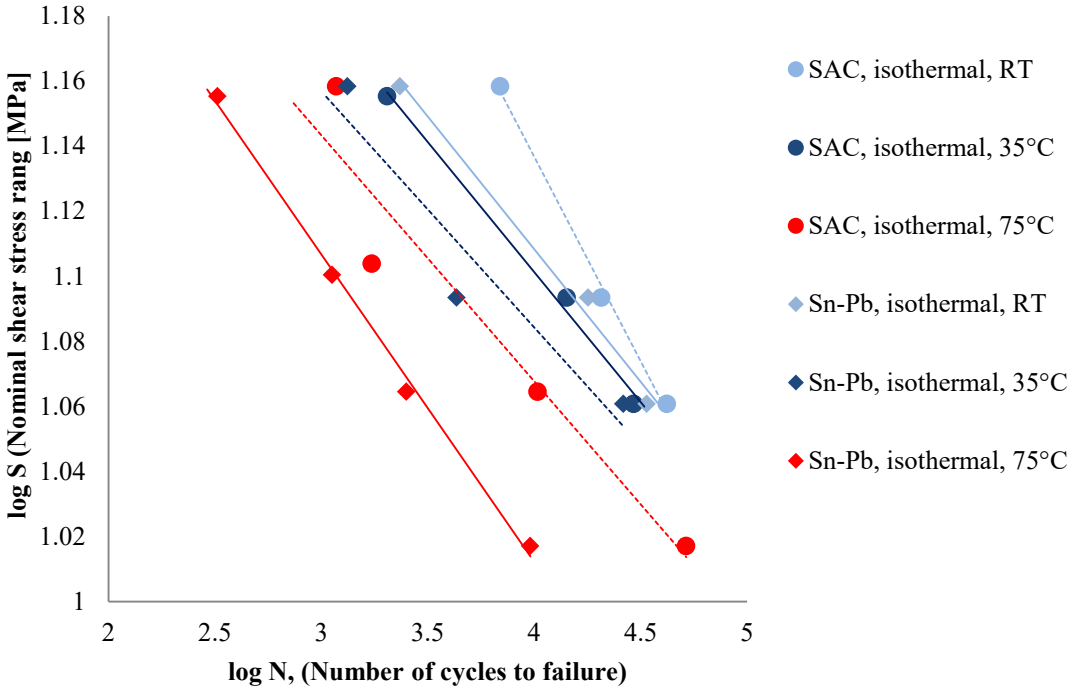

Figure 11: Stress-life behaviour for Sn-3.8Ag-0.7Cu (SAC) and Sn-37Pb (Sn-Pb) joints under isothermal mechanical fatigue loading at RT, 35°C, and 75°C.

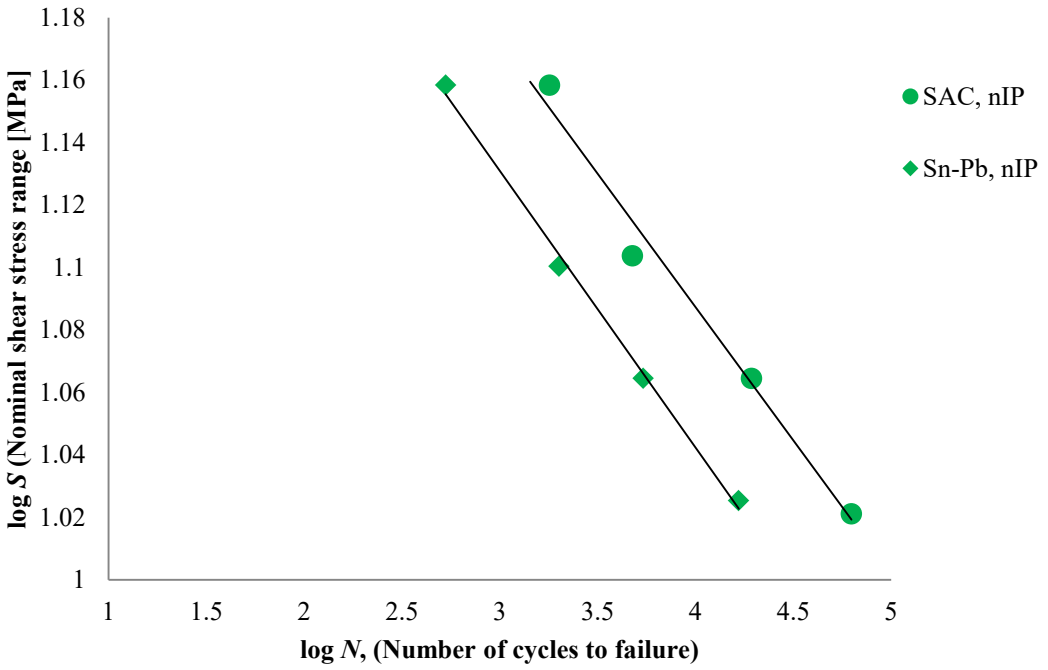

Figure 12: Stress-life behaviour for Sn-3.8Ag-0.7Cu (SAC) and Sn-37Pb joints under nIP thermo-mechanical fatigue testing (including fit lines)

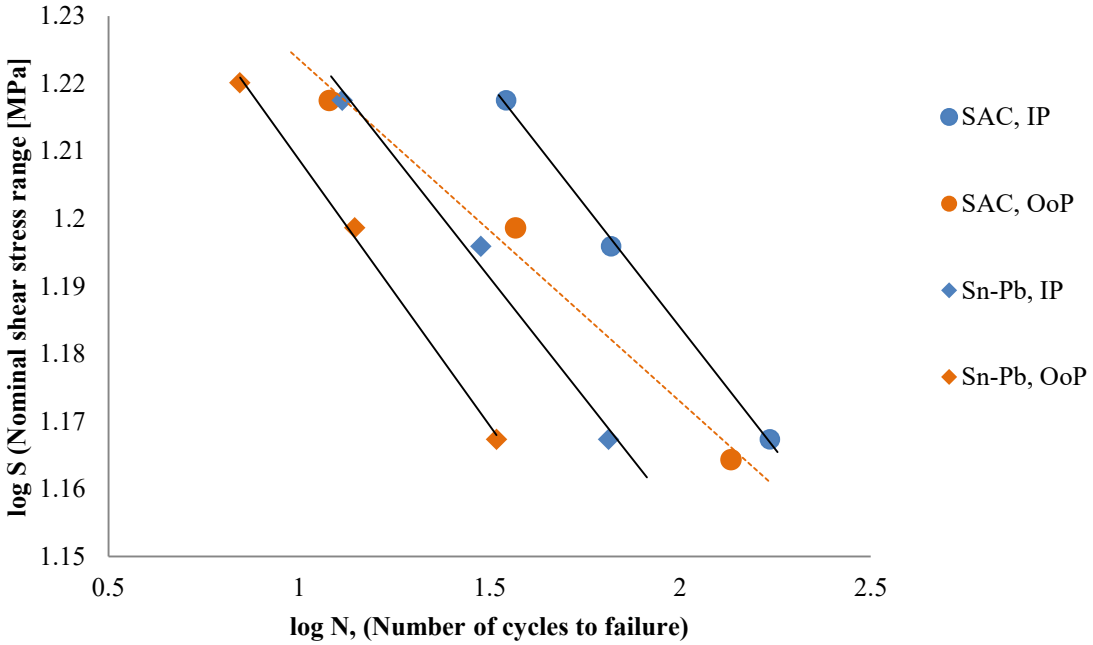

Figure 13: Stress-life behaviour for Sn-3.8Ag-0.7Cu (SAC) and Sn-37Pb under IP and OoP loading (including fit lines)

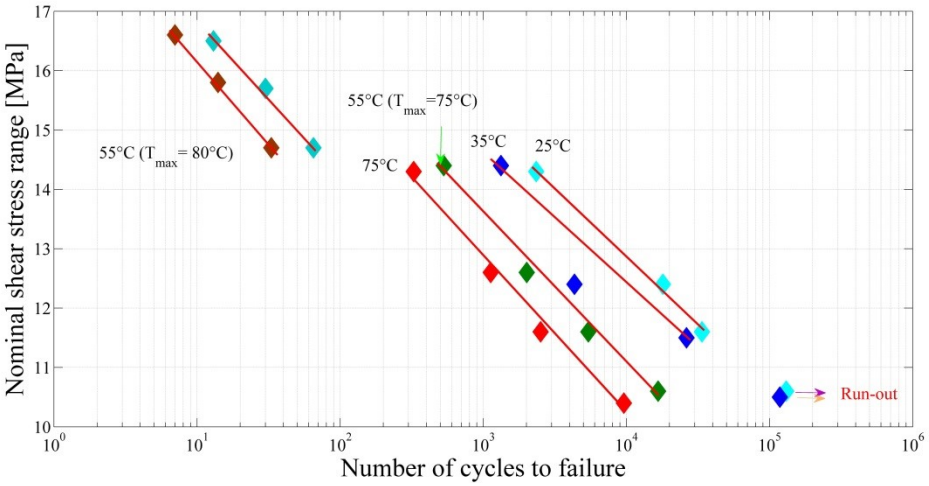

(a)

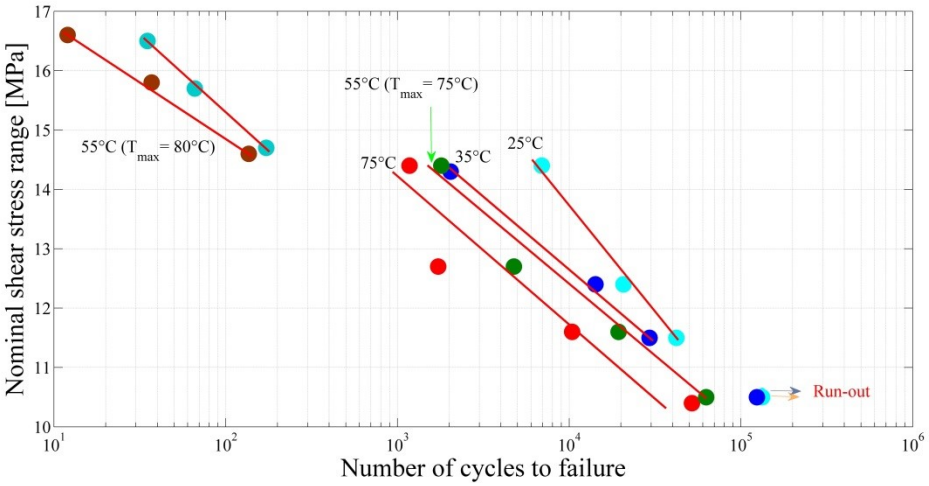

(b)

Figure 14: Comparison stress amplitude vs. number of cycles to failure for (a) leaded and (b) lead-free solder joints under isothermal mechanical and thermo-mechanical fatigue tests

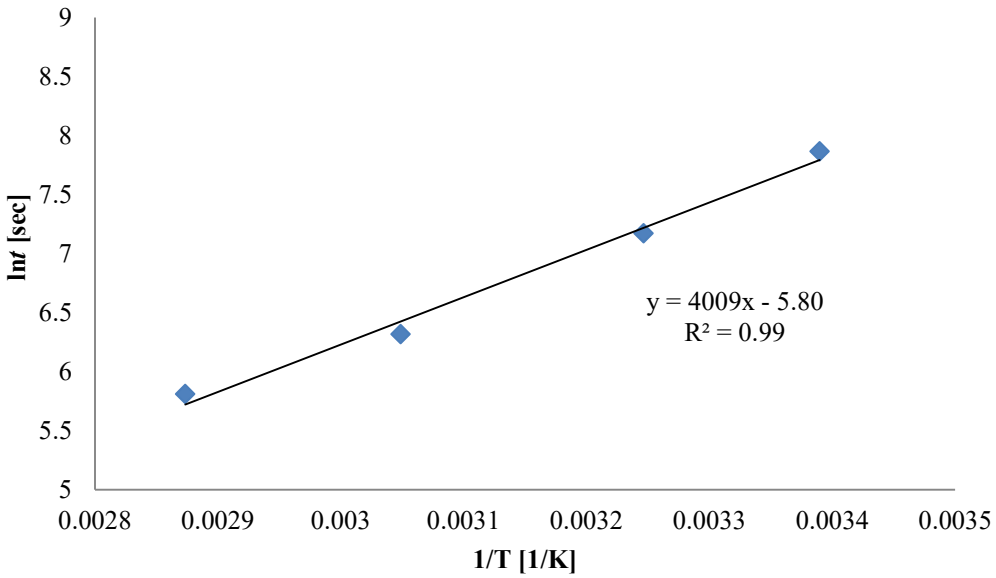

Figure 15: Arrhenius plot for time to failure at a stress range of 14.3 MPa for Sn-37Pb

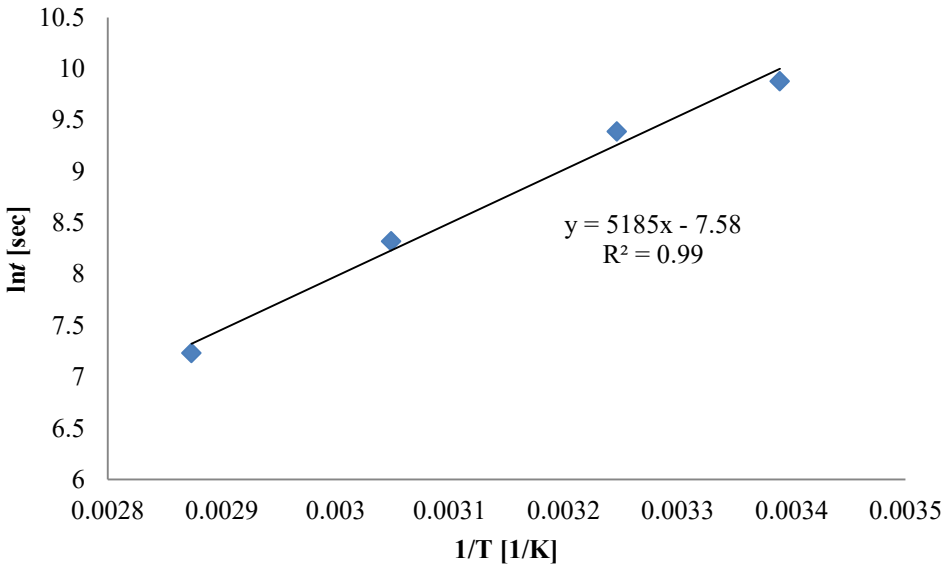

Figure 16: Arrhenius plot for time to failure at a stress range of 12.4 MPa for Sn-3.8Ag-0.7Cu

Table 1: Reflow profile parameters

Solder	**Soak**	**Peak temperature (°C)**	**Time above liquids**
Sn-37Pb	150-160 °C	220	60 s
Sn-3.8Ag-0.7Cu	150-160 °C	248	60 s

Table 2: Summary of all fatigue tests conducted in this study

Tests group	Test summary	Shear stress range [MPa]	Stress ratio	Frequency [Hz]
Isothermal tests	Each test was carried out at three different temperatures including room temperature, at 35°C and at 75°C	10.4	1.9/12.3	1.8
		11.6	2.1/13.7	1.5
		12.6	2.3/14.9	1.3
		14.2	2.4/16.6	1
nIP tests	The temperature for all tests was cycled between 35°C and 75°C and at not the same frequency of the stress cycles	10.4	1.9/12.3	1.8
		11.6	2.1/13.7	1.5
		12.6	2.3/14.9	1.3
		14.2	2.4/16.6	1
IP and OoP tests.	The temperature for all tests was cycled between 35°C and 75°C and at the same frequency of the stress cycles	14.8	2.7/17.5	0.011
		15.6	2.9/18.5	0.011
		16.5	3.2/19.7	0.011

Table 3: Constants obtained from the best fit lines of log-log stress range versus number of cycles to failure

Test conditions	*m*	*log S_1*	*S_1*	*R^2*
	Sn-3.8Ag-0.7Cu			
IF at RT	-0.1256	1.6391	43.561	0.9957
IF at 35°C	-0.08	1.4212	26.375	0.9934
IF at 75°C	-0.0756	1.3702	23.453	0.9168
nIP TMF	-0.0853	1.4286	26.828	0.9821
IP TMF	-0.0722	1.3284	21.301	0.9987
OoP TMF	-0.0507	1.2742	18.801	0.9845
	Sn-37Pb			
IF at RT	-0.0815	1.4344	26.730	0.9887
IF at 35°C	-0.0726	1.3747	23.697	0.9082
IF at 75°C	-0.0945	1.3902	24.558	0.9962
nIP TMF	-0.0886	1.3969	24.940	0.9967
IP TMF	-0.0716	1.2987	19.892	0.9894
OoP TMF	-0.0786	1.2873	19.377	0.9978